Hindawi
Advances in Materials Science and Engineering
Volume 2022, Article ID 6723396, 17 pages
https://doi.org/10.1155/2022/6723396

Research Article

Prediction Model of the Coring Asphalt Pavement Performance through Response Surface Methodology

Ekarizan Shaffie,[1,2] **Ramadhansyah Putra Jaya**,[1,3] **Juraidah Ahmad**,[2] **Ahmad Kamil Arshad**,[1] **Mohd Afiq Zihan**,[4] **and Fiona Shiong**[2]

[1]*Institute for Infrastructure Engineering and Sustainable Management, Universiti Teknologi MARA, Shah Alam 40450, Selangor, Malaysia*
[2]*School of Civil Engineering, College of Engineering, Universiti Teknologi Mara, Shah Alam 40450, Selangor, Malaysia*
[3]*Faculty of Civil Engineering Technology, Universiti Malaysia Pahang, Kuantan 26300, Pahang, Malaysia*
[4]*Detik Venture Sdn Bhd, 88 Kompleks Putra Off Jalan Gangsa, Alor Setar 05150, Kedah, Malaysia*

Correspondence should be addressed to Ekarizan Shaffie; eka@uitm.edu.my

Received 5 April 2022; Revised 18 May 2022; Accepted 24 May 2022; Published 6 July 2022

Academic Editor: Senthil Kumaran Selvaraj

Pavement evaluations provide crucial information regarding the performance and service life of asphalt concrete (HMA). They examine the structure of an existing pavement before deciding on different maintenance alternatives. The Klang Valley, as part of one of the developing areas in the state of Selangor, generates a high volume of traffic every day due to the increasing number of vehicles crossing the area. Every day, the impact of axle loads caused by vehicles has a negative impact on flexible pavement, resulting in road deterioration due to extreme distress. Pothole failures are one of the most common causes of distress. Five research areas in the Klang Valley area that have deteriorated owing to pothole failures were chosen as case studies. The objective of the study is to investigate the existing flexible pavement conditions by means of laboratory testing consisting of physical, volumetric, and performance tests using collected core samples. As a result, the data collected was compared to the Malaysian Public Work Department's (PWD) standard. Data from laboratory tests was analyzed using Response Surface Methodology (RSM) to determine correlations with parameters influencing distress. Historical data design was carried out between test components and responses, which consisted of laboratory parameters. Axial strain, tensile strength ratio, and stability were the responses measured in the RSM. The created models between the independent variables and responses revealed a high level of correlation. The binder content, degree of compaction, and stiffness were the most significant operating parameters from the 3D plots. Optimized performance due to asphaltic pavement failure was observed at binder content (5.1%), degree of compaction (97%), and stiffness (3.1 kN/mm) to achieve ultimate axial strain (5000 microstrains), tensile strength ratio (80%), and stability (9.2 kN). The study showed that the response surface methodology (RSM) is an effective statistical method for providing an appropriate empirical model for relating parameters and predicting the best performance of an asphaltic mixture to reduce flexible pavement failure.

1. Introduction

Asphalt concrete pavement is widely used across the world due to its benefits of flexibility, low cost, and ease of maintenance [1]. Flexible pavement is designed to support loads for a design life of ten to twenty years. Many related aspects, such as the pavement's structural design and environmental conditions (temperature and moisture), have an impact on its performance [2]. In Malaysia, hot mix asphalt (HMA) pavement is frequently used due to its cost-effectiveness and adaptability. Unfortunately, due to increased traffic volume, higher tire pressure, moisture, and temperature from our climatic conditions, this HMA mix has deteriorated faster than expected. Pothole failures are one of the most common causes of distress on asphalt pavement, and if not corrected promptly, they will

compromise the driver's comfort and safety. When water seeps into cracks with repeated traffic loads, the base layer weakens, and pavement structural stability can be lost quickly. The asphalt surface layer begins to deteriorate. As alligator cracking worsens, small chunks of pavement can become dislodged as vehicles drive over them. Potholes of varying sizes are then made on the pavement surface [3]. Pavement maintenance evaluations are crucial for keeping a road or highway in good condition. However, it is important to evaluate the condition of the performance and service life of existing asphalt pavement before deciding on different maintenance alternatives.

The government spends a substantial amount of money each year on road maintenance and repair, which has an indirect impact on the economy. The road condition, which was built using the conventional method, has a short lifespan and requires constant maintenance due to road defects [4]. In some cases, a number of highways even failed structurally within half a year of opening to traffic [5]. Poor construction quality has been a major contributor to this problem [5–7]. Block cracking and rutting can occur if the pavement thickness does not meet the standard, and the density is not uniformly compacted to the specified density [8]. Additionally, potholes are the result of moisture damage phenomena, along with asphalt quality and adhesion between bituminous mixtures of binder and aggregate [1, 2, 8]. Zelelew et al. investigated the structural and functional performance of the pavement at Arizona Highway in the field (destructive and nondestructive tests) and in the lab (coring samples), which revealed distress (cracking and rutting) associated with high binder content and air voids [9]. Al-Arkawazi conducted a survey to determine the type of flexible pavement failures for the selected Khanaqin-Kalar Highway, Iraq. According to his study, assessments showed that most failures in the pavement were serious and extreme surface deformation [10]. Moreover, Hosseini et al. developed a framework for connecting quality during asphalt mix production and surface construction to in-service performance through statistical correlation at the network level [11]. Rutting and alligator cracking are found to be sensitive to quality deviations in air voids, voids in mineral aggregate, and in-place density. Rutting and alligator cracking are found to be sensitive to quality deviations in air voids, voids in mineral aggregate, and in-place density. Lack of knowledge regarding the parameters affecting the asphalt performance on roads due to inexperience in the related fields has been detrimental to the quality of designed pavements, which are necessary to develop the maximum strength of asphaltic concrete mixtures. The proportion of binder in an asphalt mixture must be measured accurately in the laboratory and monitored closely at the plant. HMA with a lower asphalt binder content than required may have lower fatigue resistance and promote stripping problems [12, 13]. Whereas excess asphalt binder is an indication of high flow characteristics, it can lead to bleeding, lowered skid resistance and stability, and increased susceptibility to permanent deformation (rutting and shoving) [13–15]. The density of the degree of compaction is an important component of asphalt pavement quality and its performance. The compacted samples under a different number of Marshall compaction blows indicate that, with an increase in compaction effort, there was a consistent reduction in air void content and also an increase in both the indirect tensile strength of the mixture and its fatigue life. Excess asphalt binder, on the other hand, indicates high flow characteristics, which can result in bleeding, decreased skid resistance and stability, and increased susceptibility to permanent deformation (rutting and shoving) [12, 16]. With an increase in density and a decrease in air voids, a pavement can maintain the shape and smoothness under repeated loading [17]. However, asphalt without sufficient air entrapped in the layer will deform under traffic and result in a rutted surface [14, 17]. Meanwhile, flexible pavement constructed that contains high air voids is expected to reduce the strength. The densification can be considered as a predominant cause of rutting during initial periods of traffic, which could also lead to a greater opportunity for moisture damage [14]. The stiffness of a material is a measure of its resistance to shear loads, persistent deformation, and rutting [18]. Furthermore, the decrease in Marshall stability and the increase in flow value indicate that the asphalt mixture stiffness decreases [19].

The performance of an asphalt mixture in minimizing pavement failure may differ depending on the parameters that influence the mixing process. Using a variety of statistical and mathematical techniques, the effects of parameters on the asphalt mixture can be predicted statistically. In response to the need for the optimization of asphalt and modifier content, a statistical approach known as Response Surface Methodology (RSM) was developed to determine the optimal properties from the experimental data by using Design Expert Software. RSM is a multivariate approach technique for developing a series of experimental designs, evaluating the complex interactions of several affecting factors, and enhancing the possibilities of statistical interpretation [20, 21]. RSM is the most common design of experiment (DOE) for optimizing the operating parameters and conditions of a system [22]. Unfortunately, not many experts use this method because the researcher needs to have good statistical and numerical knowledge. The application of Response Surface Methodology (RSM) has been growing in asphalt research recently, as it not only saves time and cost, but can also predict the probability of survival of materials, which can help economically in the long run. The central composite design (CCD) method has been used along with the regression model and analysis of variance (ANOVA) [23], which considers several different factors and responses. The objective of this study is to identify existing distress in flexible pavement, which can be used as quality control in providing information for maintenance and rehabilitation methods, while performing optimization, developing models by applying Central Composite Design (CCD) based on Analysis of Variance (ANOVA), and observing the similarity of the output using Response Surface Methodology. Information from this process can be used as a guide for future construction or maintenance techniques. This study aims to investigate the effect of mixture properties on asphalt performance to minimize flexible pavement failure.

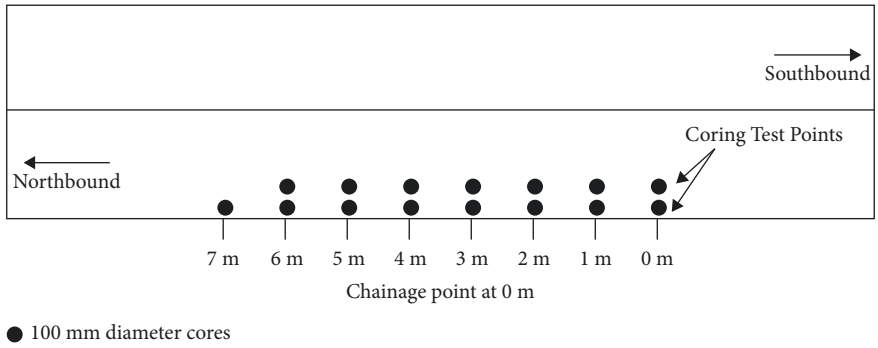

Figure 1: Typical layout of road section used during this investigation.

2. Materials and Methodology

2.1. Field Cores. Field core samples were collected from each project during construction. A total of five road locations were selected to conduct this study. Core locations were randomly stratified along the length and width of the section. The study location was chosen because the failures in the bituminous layers were mostly based on the areas exhibiting potholes failures. Causes of these failures were found to be mainly associated with the increased traffic volume. Actual locations with high volume of traffics were selected to demonstrate the pothole failure as one of the most common causes of distress in asphalt pavement in Malaysia. Developing an area that generates more traffic could lead to an increase in the traffic loading, such that the road networks in the area are extensively used by vehicles to commute between cities for various purposes or due to nature of job. For this study, the locations selected are as follows:

(i) Off Seruling 59 Road, Klang
(ii) Dato Mohd Sidin Road, Klang (Selangor state route B5)
(iii) Dato Ahmad Razali Road, Pulau Indah
(iv) Padu Road, Bukit Kemuning
(v) Jambu Road, Meru, Klang.

Figure 1 shows the normal coring positions and locations for each road segment. At each location, 15 asphalt cores were removed from locations exhibiting pothole failures. All sampling positions were maintained at the specified intervals of 1 m. For laboratory evaluation, 100 mm diameter cores were extracted from the road sections. The samples were extracted from the left wheel track of the northbound lane. A total of five cores were retained for replacement of damaged cores and repeats of laboratory tests, which provided doubtful results. The following properties were measured for each core: the theoretical maximum specific gravity of each mixture was determined in accordance with AASHTO T 209, while the bulk specific gravity was determined in accordance with ASTM D2726 and ASTM D2041, the size distribution (gradation) of the recovered aggregate according to ASTM D422. The asphalt binder content of each mixture was determined using the ignition method according to ASTM D6307; the dynamic creep test was conducted using the protocol developed by NCHRP-9-19; and the moisture susceptibility test was conducted using the Modified Lottman Test (AASHTO T283). Figure 2 shows the core samples from road sections.

Figure 2: Cores samples.

2.2. Volumetric Properties and Aggregate Gradations of Mixtures. The properties of each mixture were determined in accordance with the related standard procedure. The size distribution (gradation) of the recovered aggregate was determined in accordance with ASTM D422. The asphalt binder content of each mixture was determined using the ignition method according to ASTM D6307. The ignition method of determining asphalt binder content allows for the asphalt binder in an HMA sample to be burned off in an ignition furnace at 600°C. The degree of compaction/density analysis was determined by comparing the bulk density with the theoretical maximum specific gravity. The theoretical maximum specific gravity of each mixture was determined using AASHTO T 209, while the bulk specific gravity was determined in accordance with ASTM D2726 and ASTM D2041. Basic physical characteristics and volumetric parameters in terms of bulk specific gravity (Gmb), stability (kN), flow (mm), stiffness (kN/mm), and void in total mix (%) were determined. The Marshall stability test was conducted in compliance with ASTM D6927. The temperature of samples is controlled to 60°C either by immersion in a water bath or by placement in an oven. Load is applied at a rate of 50 mm per minute until the maximum load reading in (Newton) is obtained, and the reading on the flow meter is recorded as flow in (mm) units. Meanwhile, stiffness is

calculated using stability and flow value, whereas the void in the total mix is calculated using bulk specific gravity and theoretical maximum specific gravity, respectively.

2.3. Dynamic Creep Test. The dynamic creep test was performed in accordance with the protocol developed by NCHRP-9-19 Superpave Models, Draft Test Method W2 using a Universal Testing Machine (IPC UTM-5) using five samples from different locations [24]. It is an unconfined test that applies repeated pulsed uniaxial stress on a sample and the most used device to evaluate the permanent deformation of asphalt mixture in the laboratory. It can provide better predicted response for pavement because the dynamic or repeated loading test in laboratory can simulate the actual traffic loading. Samples were conditioned for approximately two hours before starting test to ensure that equilibrium temperature is reached. After that, the sample was inserted between the platens. The constructed platens and sample were concentrically aligned with the testing machine's loading axis. The platens are then fitted with the displacement measurement equipment. The vertical deformation is then measured by the linear variable differential transducers (LVDTs). The load was applied according to the test parameter used as shown in Table 1. The test sample was conducted until accumulated strain reaches 100,000 microstrains or until 1,800 cycles, whichever occurred first. The accumulated strain was calculated by using the following equation:

$$\varepsilon = \frac{h}{H_0}, \tag{1}$$

where ε is the accumulated strain, h is the axial deformation (mm), and ?0 is the initial sample height (mm).

2.4. Moisture Susceptibility Test. Moisture damage to hot mix asphalt (HMA) mixtures is the primary cause of HMA distress. The moisture susceptibility test was conducted, and the results can be used to predict the potential long-term stripping. Six field core samples were selected from the site for testing as control and condition samples. As a control, three samples were tested without any moisture conditioning. Three other samples were conditioned by soaking them in water until they were 70–80% wet and leaving them in a water bath at 60°C for 24 hours. The samples were then tested for indirect tensile strength (ITS) by loading the samples at a constant head rate (50 mm/minute vertical deformation at 25°C). The maximum compressive force was recorded, and the tensile strength of samples was calculated using equation (2). The potential moisture damage for core samples based on to their tensile strength ratio (TSR) was calculated using equation (3). The TSR value indicates the resistance of the mixture towards moisture damage. The retained tensile strength ratio (TSR) of 80% was used to distinguish mixtures resistant and susceptible to moisture damage [25].

$$S_t = \frac{2000P}{\pi t D}, \tag{2}$$

Table 1: Dynamic creep test parameters.

Parameters	Values
Applied pulse width duration	100 ms
Rest period before next pulse	900 ms
Stress during loading	200 kPa
Stress during rest period	10 kPa
Number of loading	1800 cycles
Temperature	40°C and 50°C

where S_t denoted tensile strength (kPa), P denoted maximum load (N), t denoted sample thickness (mm), and D denoted sample diameter (mm).

$$\text{TSR (\%)} = \left(\frac{S_{tm}}{S_{td}}\right)100, \tag{3}$$

where S_{tm} denoted average tensile strength of moisture-conditioned subset (kPa), and S_{td} denoted average tensile strength of dry subset (kPa).

2.5. Response Surface Methodology. Numerous types of design exist in RSM modelling, such as Box-Behnken, central composite designs (CCD), one factor, miscellaneous, Simplex Lattice, Simplex Centroid, screening, optimal (custom), user-defined, and historical data design. The user can define the design points based on the current experimental data. Furthermore, the historical data design has no limitation on the number of design and factor settings in comparison to other types of RSM design. The responses of an existing data set can be directly imported to a blank design layout [26]. This design was applied to evaluate the relationship between three variables and three responses in order to develop an interaction. The variables are binder content, degree of compaction (density), and stiffness, while the responses are axial strain, TSR, and stability. The experimental data were then fitted to a historical RSM design that developed into 2FI and a quadratic model, as shown in the following equation:

$$Y = \sum_{i=1}^{n} \beta_i x_i + \sum_{i=1}^{n} \beta_{ii} x_i^2 + \sum_{i=1}^{n} \sum_{j=1}^{n} \beta_{ij} x_i x_j + \varepsilon, \tag{4}$$

where Y is the model response, x represents the independent variables, and β is the regression coefficient and ε is error. β_0 is constant value, $\beta_i x_i$ and $\beta_{ii} x_i^2$ represent linear terms (first-order effects of variables) and quadratic terms (second-order effects of the variables), respectively, and $\beta_{ij} x_i x_j$ is a two-factor interaction term. This equation does not take the interaction between three factors or more into account. Equation (4) may be simplified to linear equation by setting β_{ii} and β_{ij} as 0. Moreover, a two-factor interaction (2FI) can be derived by setting β_{ii} as 0. Table 2 represents the operating factors, their designated symbols, response, and range of conditions.

An analysis of variance (ANOVA) was performed to assess the appropriateness of the proposed model. The coefficients of determination (R^2 and R^2-adj) express the wellness of the fit to the suggested model. The F-test in the program was used to determine the statistical significance of

Table 2: Design summary.

Factor	Name	Unit	Low actual	High actual	Low coded	High coded
A	Binder Content	%	3.8	8	−1	+1
B	DOC	%	94.7	98.7	−1	+1
C	Stiffness	kN/mm	1.1	5.9	−1	+1
Response	Name	Unit	Analysis	Minimum	Maximum	Ratio
Y1	Axial Strain	$\mu\varepsilon$	Quadratic	10903	96317	8.8
Y2	TSR	%	2FL	53	66	1.2
Y3	Stability	kN	Quadratic	7.3	8.5	1.2

Table 3: Sieve analysis test results.

Sieve Size (mm)	Percentage Passing						
	Sample A	Sample B	Sample C	Sample D	Sample E	Gradation Limit	
						Lower	Upper
20	100	100	100	100	100	100	100
14	97.8	97.5	93.8	97.2	97.4	90	100
10	85.0	85.7	81.1	80.1	85.4	76	86
5	58.2	55.2	52.3	50.5	54.9	50	62
3.35	46.3	47.1	44.7	43.7	46.4	40	54
1.18	24.3	28.7	28.7	28.3	28.4	18	34
0.425	12.7	16.4	16.6	16.4	16.1	12	24
0.15	7.6	7.3	8.2	7.8	7.1	6	14
0.075	4.4	4.5	4.6	4.3	4.3	4	8
Pan	0.0	0.0	0.0	0.0	0.0		

the model's adequate precision ratio (AP). After performing the F-test, the insignificant terms were identified and removed from the model. Afterwards, a finalized model based on significant variables was introduced.

3. Results and Discussion

3.1. Volumetric Properties and Aggregate Gradations of Mixtures. Table 3 summarizes the aggregate gradation mixtures from the sieve analysis tests of coring samples. Figure 3 depicts the percentage aggregate passing vs sieve size and shows the upper and lower gradation limits for all samples. The gradation for all samples was acceptable because it is close to the gradation requirements for the AC14 mix as per JKR Malaysia's specification requirements. In addition, as perceived in Figure 3, the aggregate gradation band has an S-shaped curve with significant curvature above 3.35 mm sieve, which increases permanent deformation resistance. Additionally, finer aggregate fractions, such as 0.075 mm, have the effect of filling the voids in an asphalt concrete mixture and reducing moisture infiltration.

Table 4 tabulates the results of HMA volumetric properties and degree of compaction of core samples from five locations. The average degree of compaction for all samples was lower than the minimum requirements as per Public Work Department specifications, except for samples B and E. Samples A and B achieved the highest compaction of 98%. The lower degree of compaction is indicated by a few factors such as poor mix design or poor-quality control during construction work, which resulted in nonuniformity of compaction work rate among different field sections. Even if other desirable mixture design features are met, and there is only a slight deviation from the permissible tolerance, insufficient compaction leads to poor performance. This finding is consistent with a study by previous researchers [5–8] that indicates that pavement failures can occur if the pavement thickness does not meet the standard, and the density is not uniformly compacted to the specified density. The most important determining factor in pavement performance is compaction. Poor compaction causes rutting, raveling, and moisture damage to the pavement. It also makes the pavement less stiff, reduces its fatigue life, speeds up aging, and makes it less durable. The average binder content for samples A (3.87%) was not acceptable as it was slightly lower than minimum requirements, while samples B (7.82%) and E (7.55%) exceeded minimum requirements. The asphalt binder content at the high and low levels represents the small-range binder content deviation from the target design binder content in the field as recorded. Poor mix design causes the designed binder content to be out of range for that aggregate gradation, resulting in a mixture with excessive or deficient binder content.

The Marshall stabilities and flows for tested samples are also obtained from the average of three samples. Samples C (8.09 KN) and D (8.29 kN) exhibit a stable pavement within an acceptable range (>8 kN), which maintains its shape and smoothness under repeated loading. Furthermore, although sample A has achieved high stability, it is undesirable due to insufficient asphalt binder. It can be concluded that such surfaces have low resistance to cracking. Meanwhile, samples B (7.75 kN) and E (7.79 kN) exhibit an unstable pavement due to an improper degree of both internal friction and cohesion in a mix, which allows the aggregate particles to move past each other under the imposed traffic load.

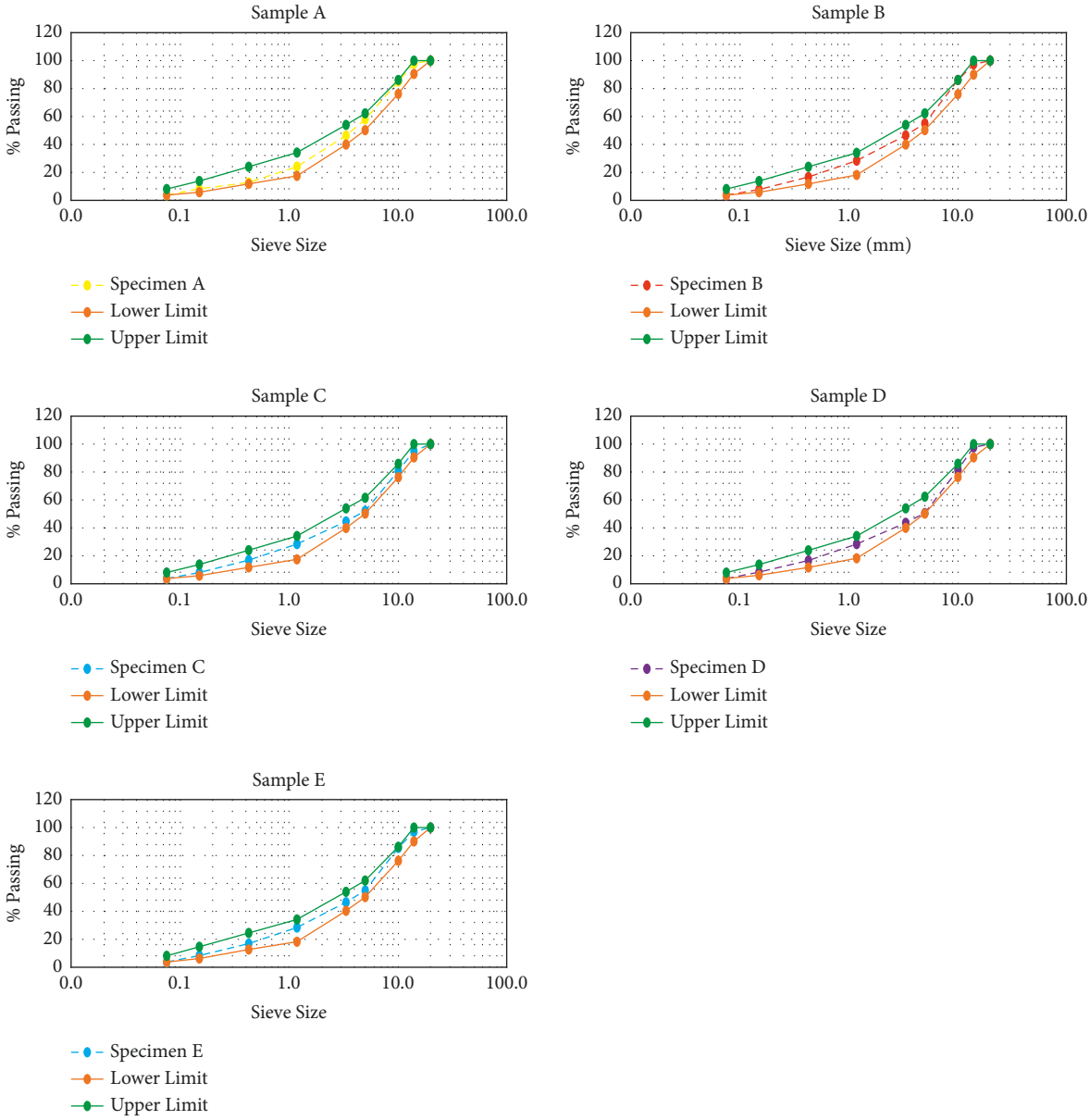

Figure 3: Aggregate gradation of coring sample.

Sample A indicates a less flexible asphalt mixture (2 mm) in terms of flow results. Meanwhile, Samples B (6.26 mm) and E (5.47 mm) achieved a high flow due to high binder content with a high tendency to be exposed to deformation (>4 mm). Although samples A achieved the highest value among all the samples, they can be concluded to exhibit the brittleness characteristic. Moreover, samples B and E showed average stiffness readings that were lower than the requirement (2 kN/mm), which can be attributed to the high flow achieved by both samples due to high binder content. Samples A achieved slightly higher air voids (3–5%), which indicates that the mix will likely be difficult to compact in the field. This can improve the permeability of the mix, allowing water to penetrate the pavement. Samples B and E have an air void content that is below the acceptable range, indicating that the mixture may be tender in the field and susceptible to rutting.

The Marshall Quotient (MQ) values are commonly used to measure the resistance of a material to shear loads and permanent deformation. The Marshall quotient is calculated by dividing the Marshall stability by the flow value. Higher MQ values indicate higher stiffness and better resistance against traffic loadings [26, 27]. The MQ value of samples A and C was higher than samples B, D, and E. As depicted in Table 4, samples A showed the highest resistance to shear stresses.

3.2. Dynamic Creep. Figure 4 illustrates the dynamic creep curve for all samples tested at 40°C and 50°C, respectively. Based on these curves, the cumulative permanent strain increases as the load cycle increases, indicating that there is a significant difference among these curves. Each dynamic

Table 4: Summary of volumetric results.

Test Property			Density Analysis		Ignition Oven	Marshall		
			Degree of Compaction (%)	Void in Total Mix (%)	Binder Content (%)	Stability (kN)	Flow (mm)	Quotient (kN/mm)
Locations	Sample A	S1	95	4.87	3.83	8.14	2.59	3.14
		S2	95	4.80	3.88	8.02	1.35	5.94
		S3	95	4.68	3.94	8.39	2.03	4.14
		S4	95	5.27	3.85	8.16	1.97	4.14
		AVG	95	4.91	3.87	8.18	1.98	4.34
	Sample B	S1	99	1.29	7.65	7.64	6.71	1.14
		S2	98	1.76	7.68	8.26	5.87	1.41
		S3	98	2.41	8.02	7.34	6.21	1.18
		S4	98	1.52	7.96	7.75	6.25	1.24
		AVG	98	1.74	7.82	7.75	6.26	1.24
	Sample C	S1	96	4.08	4.53	8.23	2.24	3.67
		S2	95	4.53	4.43	7.95	2.48	3.21
		S3	96	4.33	4.53	8.12	2.23	3.64
		S4	96	4.10	4.45	8.08	2.29	3.53
		AVG	96	4.26	4.49	8.09	2.31	3.51
	Sample D	S1	97	3.41	5.88	8.33	2.73	3.05
		S2	96	3.54	5.80	8.05	3.51	2.29
		S3	96	3.62	5.85	8.54	2.69	3.17
		S4	96	3.69	5.84	8.24	2.97	2.77
		AVG	96	3.56	5.84	8.29	2.98	2.82
	Sample E	S1	97	2.66	7.52	7.46	5.71	1.31
		S2	98	2.45	7.59	7.80	5.59	1.40
		S3	98	1.56	7.56	8.24	5.12	1.61
		S4	97	2.62	7.55	7.64	5.46	1.40
		AVG	98	2.32	7.55	7.79	5.47	1.43

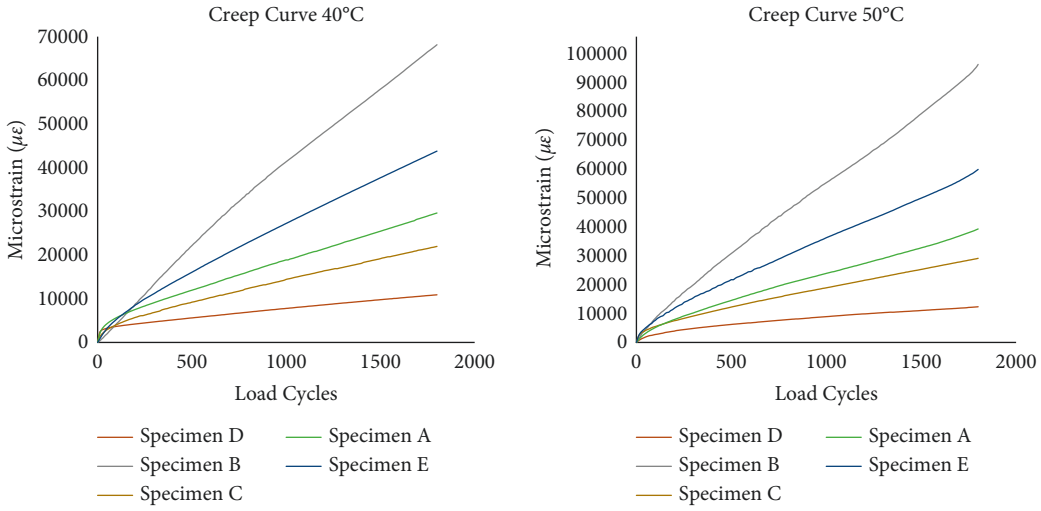

Figure 4: Dynamic creep curve at 40°C and 50°C.

creep curve consists of two parts, namely, the primary stage and the secondary stage. Due to a relatively short loading period of 1800 cycles, no sample failed during the test. Higher accumulated axial strain values indicate that mixes have lower rutting resistance potential. It is apparent that samples from different coring locations showed a substantial accumulated permanent strain. According to Iskender and Aksoy, core field samples generate greater axial strain than laboratory-prepared samples [28].

Figure 5 illustrates the results of ultimate strain after 1800 load cycles, in which the ultimate strain of all cored samples rises remarkably between two temperatures. For test conditions of 40°C, Samples B exhibited the highest ultimate strain, followed by E, A, C, and D. In addition, the same trend was observed at a 200 kPa stress level as the temperature increased. Samples B recorded the largest strain impact proportional to 6.2 and 7.8 times higher than Sample D for test conditions of 40°C and 50°C, respectively. It is

Table 5: Independent samples t-test for ultimate axial strain of coring samples.

		Levene's Test for Equality of Variances		T-Test for Equality of Means					
		F	Significant	T	DF	Sig (2-Tailed)	Mean Difference	95% CI of the Difference	
								Lower	Upper
Ultimate Axial Strain (40°C vs. 50°C	Equal Variance Assumed	1.95	0.2	−2.95	8	0.018	−124371	−221575	−27166
	Equal Variance Not Assumed			−2.95	4	0.042	−124371	−241405	−7336

important to note that the ultimate strain increases at higher temperatures. The rate of increment in strain increased, which resulted in a higher ultimate axial strain. For example, at 200 kPa stress, increasing the temperature from 40°C to 50°C for cored samples B increases the strain value from 68143$\mu\varepsilon$ to 96317$\mu\varepsilon$, which is 1.41 times higher than at 40°C. It can be concluded that as the temperature increases, cored samples deform significantly. It leads to a huge increase in the ultimate strain of samples B and E, resulting in the destruction of these samples approaching 100,000 $\mu\varepsilon$.

In addition, an independent t-test analysis was performed to determine the effects of temperature on the ultimate axial strain. The null hypothesis is that the ultimate axial strain at 40°C and 50°C is equal (Ho: μ40 strain = μ50 strain). Levene's test for equality of variances indicates that the population variance is equal; hence, the t-value is used to test the null hypothesis based on Table 5. The results show that the two-tailed significance level is 0.018; hence, the null hypothesis is rejected. This indicates that the mean difference between ultimate axial strain at 40°C and 50°C is significant. Because of this, the increase in temperature has an effect on the increase in ultimate axial strain.

The creep stiffness value is an additional indicator of the resistance to permanent axial deformation. Creep stiffness can be calculated by the following equation:

$$CS = \frac{\sigma_o}{\varepsilon\left(40^{\circ}C, curve3/3\right)}, \quad (5)$$

where ε (40°C, curve$^{3/3}$) denotes the axial strains after full load cycles, and σ_o is the applied stress = 200 kPa. As proven by this study, samples B and E, which achieved higher ultimate axial strain, recorded lower creep stiffness among other samples, as depicted in Figure 5. Moreover, according to [29], increasing the temperature has significant effects on creep stiffness. The creep stiffness at 50°C test condition is approximately at least 12% lower compared to the corresponding values of samples for 40°C condition. Figure 6 illustrates that, for all samples tested at elevated temperatures, the creep stiffness decreases, while cumulative strain increases.

A t-test statistical analysis was also conducted to determine the effects of temperature on the ultimate axial strain (Ho: μ40 stiffness = μ50 stiffness). From Table 6, the

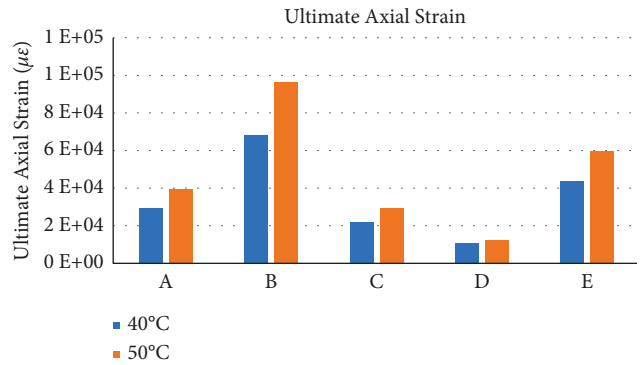

Figure 5: Ultimate axial strain of coring sample.

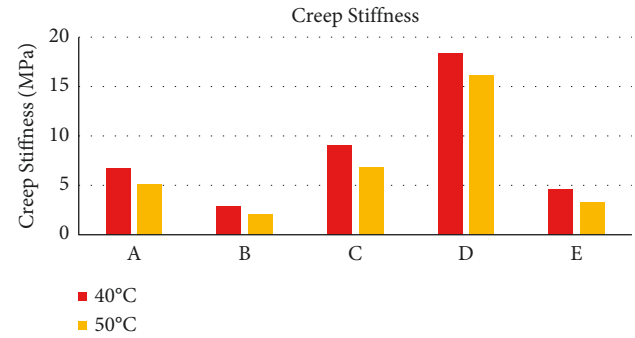

Figure 6: Creep stiffness of coring samples.

results of Levene's test for equality of variances show that the t-values = 0.529, which is considered to test for the null hypothesis. The results showed that the p-value for the T-Test is 0.035, less than 0.05; hence, the null hypothesis is rejected. This indicates that the mean difference between creep stiffness at 40°C and 50°C is significant. Thus, there was a substantial change in creep stiffness at elevated temperatures.

The Creep Strain Slope (CSS) is defined as the slope of the secondary stage based on two linear fittings from the dynamic creep curve, which results in a logarithmic plot of strain versus load cycle. If axial strains (in microstrains) are

Table 6: Independent samples *t*-test for ultimate axial strain of coring samples.

		Levene's Test for Equality of Variances		*T*-Test for Equality of Means					
		F	Significant	*T*	DF	Sig (2-Tailed)	Mean Difference	95% CI of the Difference	
								Lower	Upper
Creep Stiffness (40°C vs. 50°C)	Equal Variance Assumed	0.43	0.529	2.53	8	0.035	8.04	0.70	15.38
	Equal Variance Not Assumed			2.53	6	0.045	8.04	0.26	15.83

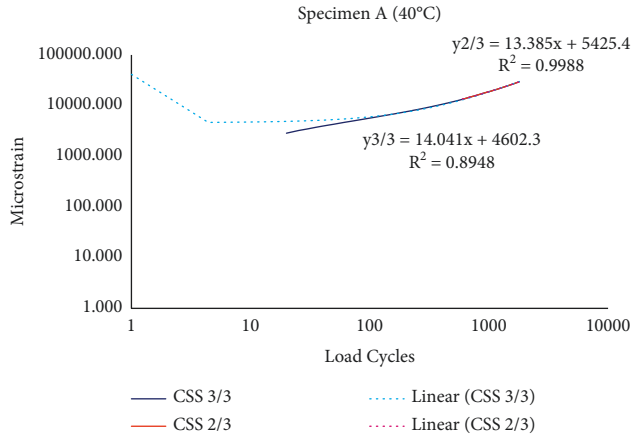

Figure 7: Intercept of two-fittings.

depicted in the plot of log strain versus log load cycles, all strains still exhibit a curve relationship with load cycles. Based on Figure 7, the dynamic creep curve consists of two parts that represent the densification of the mixture during the test at the nonlinear segment and the stable development of axial strain in the linear segment of the curve. From the in-depth analysis tabulated in Table 7, a linear relationship with a higher coefficient was achieved for the linear relationship between axial strain and load cycles after 600 cycles. The relationship coefficient is small when this curve is linearly fitted [30]. As a result, this plot is divided into two segments to allow for analysis of densification, characteristic under load repetition, and the mixture's susceptibility to permanent deformation.

Permanent deformation at the densification stage can be roughly represented by the initial axial strain derived from the intercept of the fitted linear equation based on the dynamic creep curve. A larger intercept signifies a higher initial permanent deformation. The initial permanent deformation of a sample is not caused by load cycles but is influenced by method and mix grading. The accuracy of the fitted linear equation denoted by the coefficients of determination (R^2) expresses the wellness of the fit to the suggested model. From the Table 7, R^2 of both fitted linear equations of CSS3/3 and CSS2/3 for samples B and D, respectively, indicated a value nearly to 1, which proved a high level of correlation. Furthermore, R^2 at CSS2/3 for samples B and D, respectively, shows an improvement compared to R^2 for the whole slope of linear dynamic creep curve (CSS3/3). With regard to CSS findings that were mentioned before, this further proved that CSS2/3 is more accurate in determining the characteristics of permanent deformation reflected by the trend of axial strain. At 50°C, sample B shows a larger intercept, which indicates high initial permanent deformation at the densification stage compared to sample D. The least deformed mix at the initial densification stage is Specimen D.

The results of the densification pattern of the samples are plotted in Figure 8. At 50°C, all of the samples have a larger intercept, which means that there was more permanent deformation at the beginning of the densification stage than at 40°C.

However, further evaluation to characterize permanent deformation must be done at the other two-thirds part of the linear dynamic creep curve in the logarithmic plot known as the creep strain slope (CSS). Furthermore, the slope of the last two-thirds of the dynamic creep curve in the log–log plot, namely, creep strain slope (CSS2/3), reflects the trend of axial strain. As CSS 2/3 excludes initial permanent deformation, CSS was employed to assess the susceptibility of the mixtures to the permanent deformation under load repetitions as it offers characterization of the permanent deformation on the other two-thirds of the linear dynamic creep curve. Similarly, B recorded a higher CSS compared to D, which denoted a high susceptibility to permanent deformation.

An asphalt mixture less resistant to permanent deformation can be denoted by a higher CSS 2/3 [31]. In the subsequent context, CSS 2/3 is replaced with CSS, in microstrain per cycle. The CSS can be calculated using the following equation:

$$CSS = \frac{\log\varepsilon_{(40^{\circ}C,curve^{3/3})} - \log\varepsilon_{(40^{\circ}C,curve^{2/3})}}{\log cycle_{(40^{\circ}C,curve^{3/3})} - \log cycle_{(40^{\circ}C,curve^{2/3})}}, \quad (6)$$

where ε (40°C, $curve^{2/3}$) and ε (40°C, $curve^{3/3}$) denote the axial strains at the two-thirds of load cycle and full load cycles, respectively. A similar trend can be observed when test temperature is raised by 10°C, with samples C achieving the lowest increase in creep strain slope followed by samples D with increment by 2.38%. This in general designates that both samples C and D are the most resistant to permanent deformation among all samples.

In addition, Figure 9 illustrates the relationship between ultimate strain and CSS. Pearson Correlation was used to

Table 7: Fitted linear relationship of the dynamic creep curve.

Temperature	Fitted Linear Relationship for Dynamic Creep Curve	R^2	Linear Relationship for 2/3 Dynamic Creep Curve	R^2
Sample A				
40°C	$y^{3/3} = 14.041x + 4602.3$	0.8948	$y^{2/3} = 13.385x + 5425.4$	0.9988
50°C	$y^{3/3} = 19.398x + 4180.9$	0.8943	$y^{2/3} = 18.15x + 5756.9$	0.9887
Sample B				
40°C	$y^{3/3} = 37.403x + 2622.4$	0.8957	$y^{2/3} = 34.178x + 6808.3$	0.9794
50°C	$y^{3/3} = 50.094x + 4732.1$	0.8983	$y^{2/3} = 48.513x + 6720.4$	0.9118
Sample C				
40°C	$y^{3/3} = 10.529x + 3553.8$	0.8915	$y^{2/3} = 9.7291x + 4566$	0.9894
50°C	$y^{3/3} = 13.823x + 4825.9$	0.8924	$y^{2/3} = 12.769x + 6161.3$	0.9799
Sample D				
40°C	$y^{3/3} = 4.3611x + 3309.1$	0.8838	$y^{2/3} = 4.0347x + 3722.6$	0.9992
50°C	$y^{3/3} = 5.5521x + 3004.9$	0.7632	$y^{2/3} = 4.4863x + 4362.9$	0.9352
Sample E				
40°C	$y^{3/3} = 22.568x + 4164.8$	0.8953	$y^{2/3} = 21.057x + 6088.2$	0.9898
50°C	$y^{3/3} = 29.745x + 5945.7$	0.8664	$y^{2/3} = 28.407x + 7620.9$	0.9594

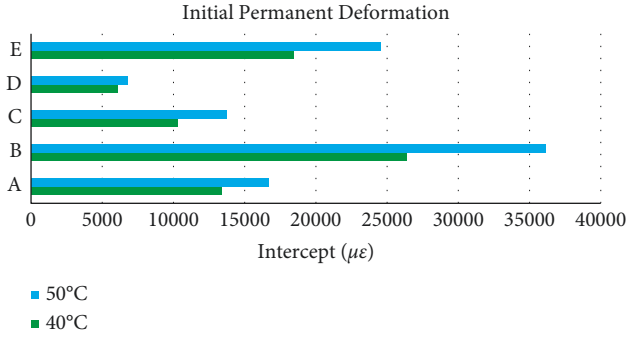

Figure 8: Initial permanent deformation.

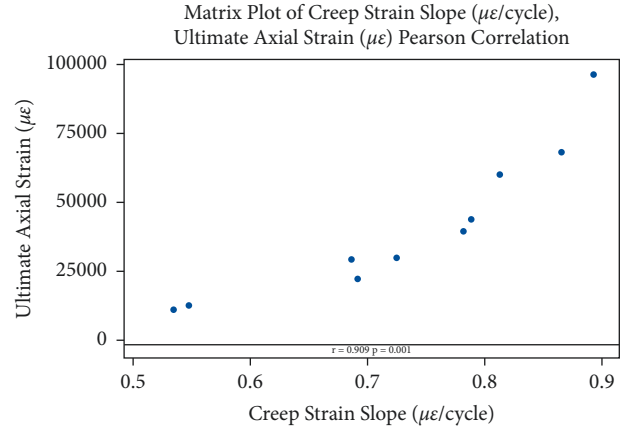

Figure 9: Matrix plot of Pearson correlation (ultimate axial strain vs CSS).

evaluate the relationship between the variables. There was a strong positive correlation between CSS and axial strain, $r = 0.909$, p-Value = 0.001. A strong correlation means that CSS increases with an increase in the axial strain. Therefore, if the creep strain slope of the mix is enhanced, then the susceptibility to permanent deformation will increase consequently. Thus, ultimate strain and CSS are considered to be useful parameters for evaluating the permanent deformation susceptibility of the mixtures.

The dynamic creep stiffness modulus is defined as the ratio of applied stress to total axial strain caused by specific load cycles at testing temperature. Nevertheless, due to the initial axial strain that occurred during the densification process at the initial stage, actual permanent deformation of samples cannot be precisely determined. As a result, the dynamic creep stiffness modulus can not reflect the susceptibility of the permanent deformation only caused by repeated loading. Consequently, to describe the permanent deformation under the loading at the stable development stage of the dynamic creep test, the data in the last two-thirds of the curve is used to calculate the secant creep stiffness modulus (SCSM). SCSM can be calculated by the following equation:

$$SCSM = \frac{\sigma_o}{\varepsilon_{(40^\circ C, curve^{3/3})} - \varepsilon_{(40^\circ C, curve^{2/3})}}, \quad (7)$$

where ε (40°C, curve$^{2/3}$) and ε (40°C, curve$^{3/3}$) denote the axial strains after two-thirds of a load cycle and full load cycles, respectively, and $\sigma_o = 200$ kPa is the applied stress. The resistance of the mixtures to permanent deformation with respect to secant stiffens creep modulus is shown in Figure 9. As shown in Figure 10, the SCSM ranged from 47.8 MPa to 413.3 MPa at 40°C, which was relatively low. Meanwhile, SCSM decreases further with a temperature increase of 10°C, ranging between 33.2 MPa and 358.4 MPa. At both test temperatures, samples D achieved the highest SCSM, whereas samples B recorded the lowest value of SCSM.

The relationship between SCSM and CSS is delineated in Figure 11. There was a strong correlation between SCSM and CSS; $r = 0.954$, p-Value = 0.001. A strong correlation means that CSS decreases with an increase of SCSM. Therefore, enhancing SCSM will minimize the susceptibility of a mixture to permanent deformation.

3.3. Moisture Susceptibility. The moisture susceptibility of HMA mix was conducted to determine the sensitivity of mixture to moisture. The indirect tensile strength test is used to determine the tensile properties of the asphalt pavement,

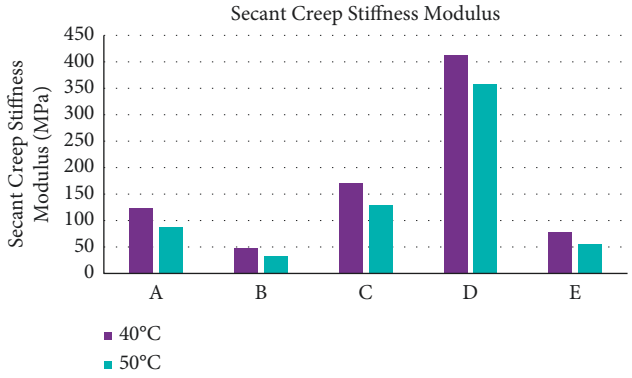

Figure 10: Secant creep stiffness modulus of coring samples.

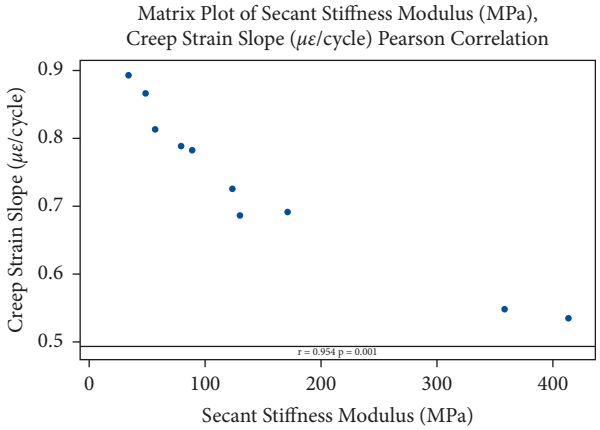

Figure 11: Matrix plot of Pearson correlation (CSS vs SCSM).

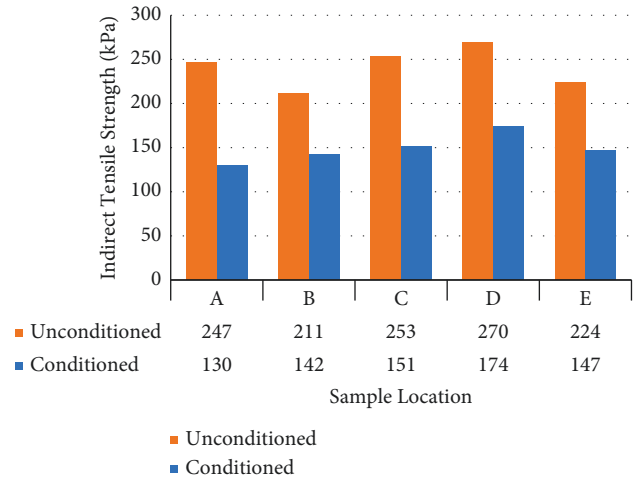

Figure 12: Indirect tensile strength (ITS) of coring samples.

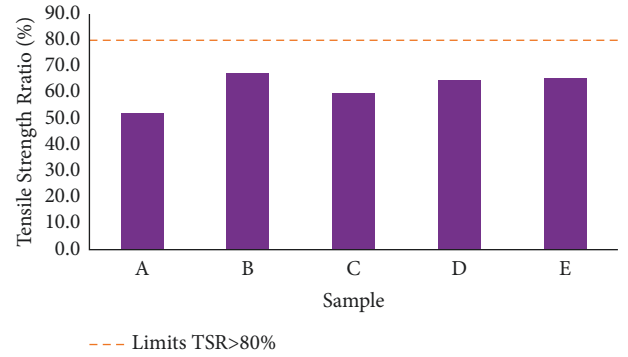

Figure 13: Tensile strength ratio (TSR) of coring samples.

which can be further related to the cracking properties of the pavement. Figure 12 illustrates the average indirect tensile strength (ITS) for asphalt samples. The result indicates that the unconditioned sample shows higher values of tensile strength compared to conditioned samples. It shows that the moisture decreased the value of indirect tensile strength. This outcome signifies that there was a deterioration in the mixtures, which affected the strength of the HMA mixes and thus reduced the tensile strength of the mixtures. Compared to HMA with a low tensile strain at failure, HMA that has a higher tensile strain at failure can resist higher strains before failing and increase resistance to cracking. If the unconditioned tensile strength is relatively low compared to the conditioned tensile strength, the asphaltic mixture can be regarded as practically resistant to moisture. The results suggest that the tensile strength of sample D increases significantly under both conditions.

The tensile strength ratio (TSR) result is an indication of whether the asphaltic mix is susceptible to moisture damage. A TSR of 0.8 or above has typically been used as a minimum acceptable value for hot mix asphalt. Mixtures with a tensile strength ratio of less than 0.8 are prone to moisture damage, and mixtures with a ratio greater than 0.8 are relatively resistant to moisture damage [32]. Figure 13 clearly demonstrates that the ratio of tensile strength for all samples was less than 80%, indicating that all samples were susceptible to moisture damage. In the presence of water, internal bonding between aggregate and asphalt binder was poor in all pavement core samples. It may be due to poor absorption of the binder that is needed to coat the aggregate, thus reducing the stripping resistance. The statistical independent *T*-Test was performed to further validate the effect of moisture content on tensile strength. Table 8 demonstrates that the two-tailed significance level is 0.001; hence, the null hypothesis is rejected. This shows that the mean difference between conditioned and dry samples was statistically significant. Thus, there was a substantial change in tensile strength due to moisture.

3.4. Historical Data Design. Twenty sets of experiments were selected as design points to develop a regression model for the results. The experimental data range was used to establish minimum and maximum values for variables and responses. The experimental matrix is provided in Table 9. Regression analysis was performed using the historical data design to fit the response function. The model was improved by manual reduction, which involved the elimination of larger insignificant terms.

Table 10 presents the details of the proposed model for responses. According to the ANOVA result, which was constructed based on the Two-Factor Interaction (2FL) and

Table 8: Independent samples t-test for ultimate axial strain of coring samples.

		Levene's Test for Equality of Variances		T-Test for Equality of Means					
		F	Significant	T	DF	Sig (2-Tailed)	Mean Difference	95% CI of the Difference	
								Lower	Upper
Moisture Susceptibility (Conditioned vs. Dry)	Equal Variance Assumed	0.62	0.455	−5.25	8	0.001	−96.5	−138.8	−54.1
	Equal Variance Not Assumed			−5.25	7	0.001	−96.5	−139.9	−53.1

Table 9: Experimental matrix for historical data design.

Std.	Run	Factor 1 A:Binder Content %	Factor 2 B:Degree of Compaction %	Factor 3 C:Stiffness kN/mm	Response 1 Ultimate Axial Strain $\mu\varepsilon$	Response 2 Tensile Strength Ratio %	Response 3 Stability kN
9	1	5.9	96.3	2.3	10903	65	8.5
11	2	5.8	96.6	3.2	10903	60	8.1
3	3	3.9	95.3	5.9	96317	53	8.4
16	4	5.8	96.5	2.8	12355	60	8.2
21	5	8.0	97.6	1.4	96317	67	7.3
18	6	3.9	95.2	4.1	39312	60	8.0
10	7	4.5	95.9	3.6	29150	65	8.1
4	8	4.5	95.7	3.7	21983	60	8.2
6	9	7.7	98.5	1.2	68143	67	8.3
17	10	8.0	98.7	1.2	68143	65	7.8
2	11	5.9	96.4	3.0	21983	53	8.3
7	12	7.5	97.4	1.6	43790	66	7.6
26	13	7.6	97.3	1.3	59936	66	7.8
14	14	4.4	95.5	3.2	12355	65	8.1
15	15	7.6	98.4	1.4	59936	66	8.2
25	16	3.8	94.7	3.1	29625	53	8.2
20	17	7.8	98.2	1.1	43790	67	7.6
24	18	4.5	95.9	3.5	29150	67	8.0
13	19	3.9	95.1	4.0	39312	53	8.1
19	20	7.6	97.6	1.4	29625	66	7.5

Quadratic model, the p-value was less than 0.05. The F-values for the models are 63.07, 19.10, and 71.58, respectively, indicating that all models are significant with a probability of only 0.01%. This indicates that the models represent data within the 95% confidence interval (CI). The 95% confidence interval ($p < 0.05$) could be used to determine the significance of all the models and their terms. The results also indicate that all the models have a high degree of correlation (R^2), implying experimental values of stability values of just 3.29%, 14.89%, and 2.90%, respectively. The difference between the adjusted degree of correlation (Adj. R^2) and predicted degree of correlation (Pred. R^2) for all the models was less than 0.2, indicating that the Adj. R^2 and Pred. R^2 were in reasonable agreement. Also, the adequacy precision (AP) values for each model were greater than 4, which means that each model can be used to explore the design space.

Figure 14 depicts a diagnostic plot that was used to determine the adequacy of the regression model between the experimental data and the model response. The regression line yielded adjusted R^2 values of 0.9671, 0.8511, and 0.9710, as well as the predicted R^2 values of 0.8785, 0.7268, and 0.8620. Both statistical R^2 values demonstrated a strong correlation between the predicted and actual experimental response values. It can be observed that the 2FI and quadratic regression models fit realistically, thereby adequately expressing the experimental range studied.

Figure 15 displays the graphical analysis of the model as depicted by the normal plot of residuals. It is obvious that the residuals reflect a normal distribution since virtually all the points follow a straight-line curve. It is also revealed that no further improvement can be made to the model by modification of response due to scattered data points, which inhibit "S-shaped" curve [28].

Table 11 shows the results of ANOVA, which was used to analyze the adequacy of the model. The p-value of less than 0.005 indicates that the terms are significant. Factor A (binder content) had the greatest effect on axial strain, since the majority of the equations incorporating this factor had the lowest p-value. Furthermore, the combined effect of the

Table 10: Model proposed for RSM.

Response	Description	Sum of Squares	Degree of Freedom	Mean Square	*F*-Value	Prob > F	Model
Axial Strain	Regression	$1.282E+10$	9	$1.425E+09$	63.07	<0.0001	Quadratic
	Residual Error	$2.259E+08$	10	$2.259E+07$			
	R^2	0.9827					
	Adjusted R^2	0.9671					
	Predicted R^2	0.8785					
	Standard Deviation	4752.63					
	Mean	41151.40					
	Adequate Precision	26.7561					
Tensile Strength Ratio	Regression	$5.008E+02$	6	$8.347E+01$	19.10	<0.0001	2FI
	Residual Error	$5.681E+01$	13	$4.370E+00$			
	R^2	0.8981					
	Adjusted R^2	0.8511					
	Predicted R^2	0.7268					
	Standard Deviation	2.09					
	Mean	62.42					
	Adequate Precision	13.4484					
Stability	Regression	$1.820E+00$	9	$2.023E-01$	71.58	<0.0001	Quadratic
	Residual Error	$2.825E-02$	10	$2.825E-03$			
	R^2	0.9847					
	Adjusted R^2	0.9710					
	Predicted R^2	0.8620					
	Standard Deviation	0.0532					
	Mean	8.02					
	Adequate Precision	32.5658					

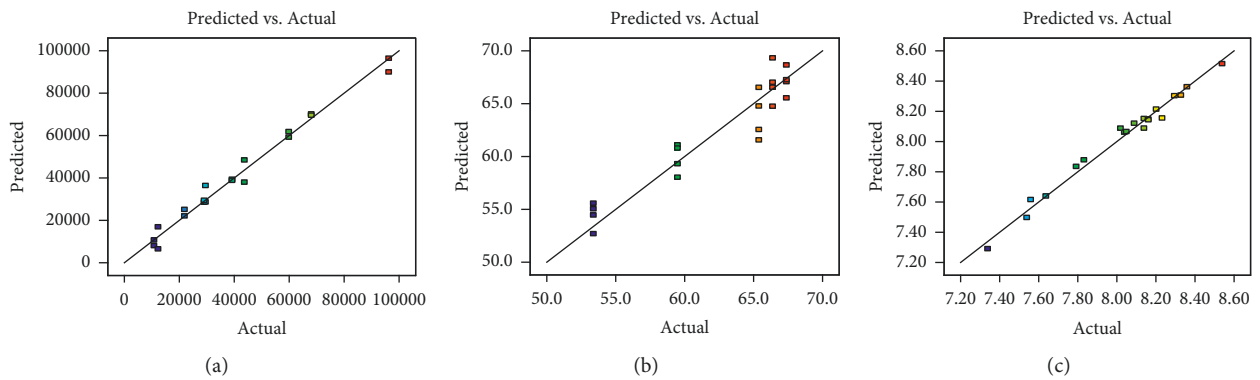

Figure 14: Cross plot between the predicted and experimental values. (a). Axial strain, (b). TSR, (c). Stability.

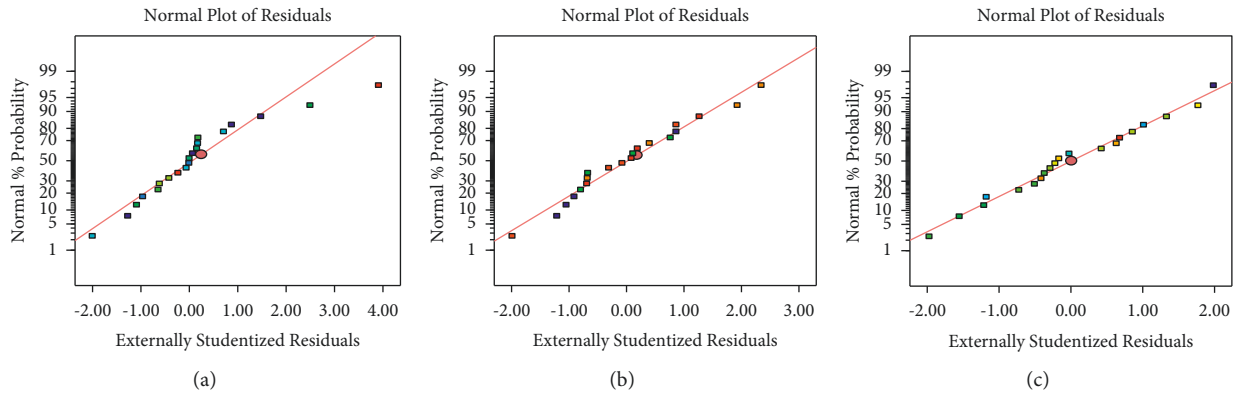

Figure 15: Normal plot of residuals for the model. (a). Axial strain, (b). TSR, (c). Stability.

Table 11: ANOVA analysis for response model.

Response	Factor	Sum of Squares	Degree of Freedom	Mean Square	F-value	Prob > F
Axial Strain	A-Binder Content	$2.280E+08$	1	$2.280E+08$	10.09	0.0099
	B-Degree of Compaction	$1.277E+08$	1	$1.277E+08$	5.65	0.0388
	C-Stiffness	$4.142E+08$	1	$4.142E+08$	18.34	0.0016
	AB	$1.471E+09$	1	$1.471E+09$	65.13	<0.0001
	AC	$2.226E+08$	1	$2.226E+08$	9.85	0.0105
	BC	$2.497E+08$	1	$2.497E+08$	11.06	0.0077
	A^2	$1.289E+09$	1	$1.289E+09$	57.09	<0.0001
	B^2	$1.384E+09$	1	$1.384E+09$	61.27	<0.0001
	C^2	$1.557E+08$	1	$1.557E+08$	6.89	0.0253
Tensile Strength Ratio	A-Binder Content	$1.951E+02$	1	$1.951E+02$	44.65	<0.0001
	B-Degree of Compaction	$8.847E+01$	1	$8.847E+01$	20.24	0.0006
	C-Stiffness	$6.085E+01$	1	$6.085E+01$	13.92	0.0025
	AB	$7.679E+00$	1	$7.679E+00$	1.76	0.2078
	AC	$1.327E+02$	1	$1.327E+02$	30.36	0.0001
	BC	$4.506E+01$	1	$4.506E+01$	10.31	0.0068
Stability	A-Binder Content	$4.415E-03$	1	$4.415E-03$	1.56	0.2398
	B-Degree of Compaction	$2.078E-02$	1	$2.078E-02$	7.35	0.0219
	C-Stiffness	$7.301E-02$	1	$7.301E-02$	25.84	0.0005
	AB	$1.855E-01$	1	$1.855E-01$	65.66	<0.0001
	AC	$3.334E-04$	1	$3.334E-04$	0.12	0.7383
	BC	$1.756E-02$	1	$1.756E-02$	6.22	0.0318
	A^2	$3.152E-02$	1	$3.152E-02$	11.16	0.0075
	B^2	$2.832E-01$	1	$2.832E-01$	100.24	<0.0001
	C^2	$1.024E-03$	1	$1.024E-03$	0.3624	0.5606

two components was considerable, implying that all terms are interdependent in influencing the characteristics of axial strain. Factor AB (tensile strength ratio (TSR)) is greater than 0.05, indicating that the factor binder content and degree of compaction have no interaction and are independent of one another. In the quadratic model, A, AC, and C2 were insignificant factors and interactions for stability response. However, the combined effect of the two factors (AB and A^2) was significant to the model development. In the meantime, combining the effects with component C resulted in insignificant factors. The model factors and their interactions were assigned negative and positive signs to indicate the antagonistic or synergistic effects of the variables on the performance of asphalt mixes. The models for the axial strain, TSR, and stability of asphalt mixtures comprising all the terms are shown in equations (8)–(10), respectively:

$$Y\text{strain} = 85869.26 + 1760.41A - 1899.58B + 559.69C - 19.54AB + 5.62AC6.18BC + 9.70A^2 + 10.51B^2 + C^2, \quad (8)$$

$$Y\text{tsr} = 1884.95 + 12.19A - 19.42B - 1281.58C - 10.24AC + 13.82BC, \quad (9)$$

$$Y\,stabilit\,y = 14284.9 + 232.21A - 310.83B + 55.97C - 2.47AB - 0.58BC + 0.54A\hat{2} + 1.69B\hat{2}, \quad (10)$$

where A, B, and C are parameters representing binder content, degree of compaction, and stiffness, respectively.

Three-dimensional (3D) response surface plots were used to illustrate the impact of interactions between independent factors and response variables. As shown in Figure 16, axial strain increased as the binder content increased. On the other hand, an increase in stiffness results in a reduction of axial strain. Meanwhile, the interaction between the degree of compaction and axial strain showed a different effect. Reduction of the degree of compaction lower than 96% can increase axial strain. Similarly, axial strain increased when compaction exceeded 98%. However, as compared to compaction effort and stiffness, the influence of binder content is more significant, as indicated by the red zone (highest value) at high binder concentration. In conclusion, excessive binder can result in high susceptibility to deformation.

Figure 17 illustrates the response surface model for tensile strength ratio (TSR). A linear relationship can be observed between independent variables and response. Changes in binder content, degree of compaction, and stiffness can have a big effect on the TSR, as shown by the red and blue regions. The highest TSR value was produced as a result of a rise in the content of independent variables, whereas the least TSR value resulted from a reduction in binder content, degree of compaction, and stiffness.

Based on the quadratic model from Figure 18, an increase in the degree of compaction and stiffness can increase

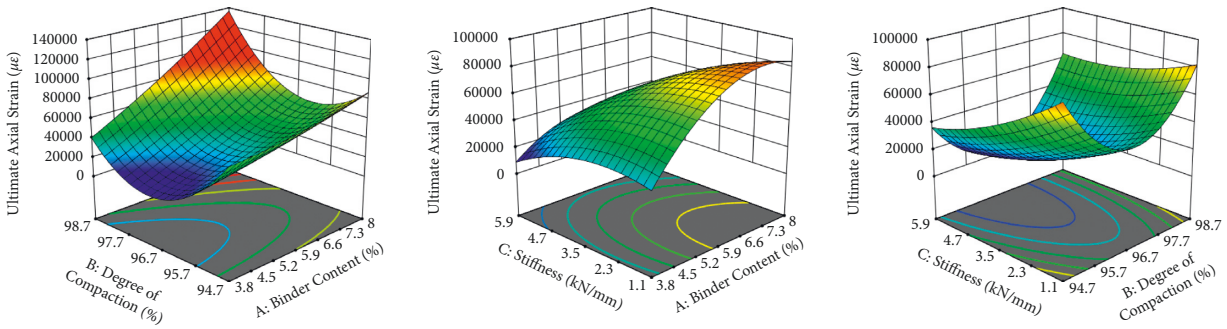

Figure 16: Response surface model of axial strain.

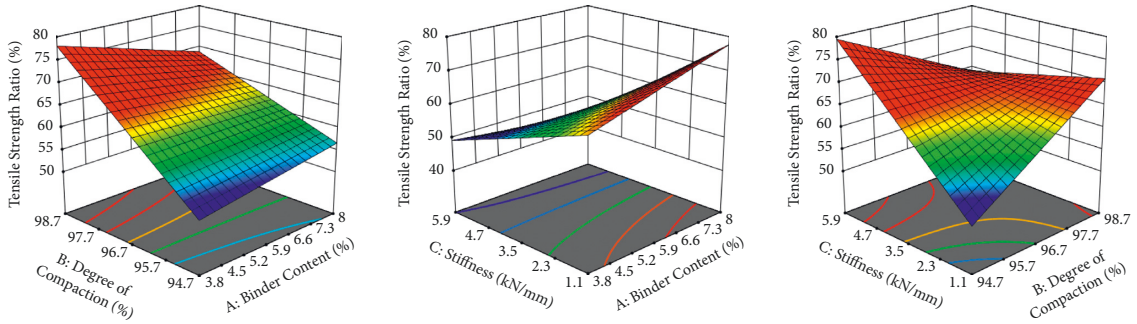

Figure 17: Response surface model for tensile strength ratio.

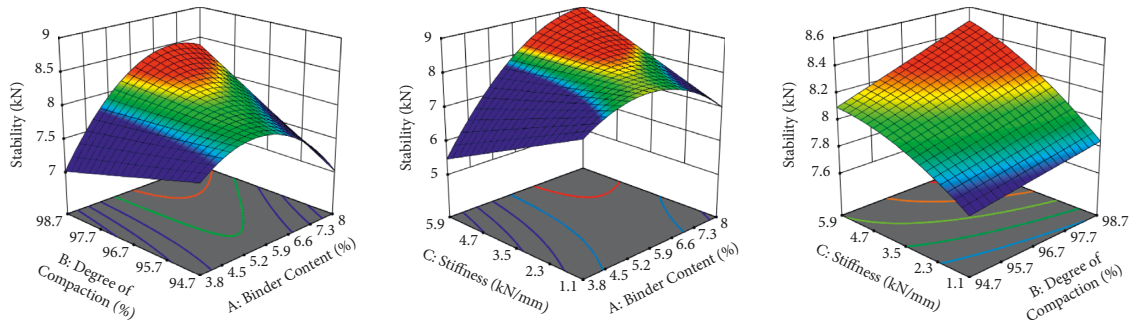

Figure 18: Response surface model for stability.

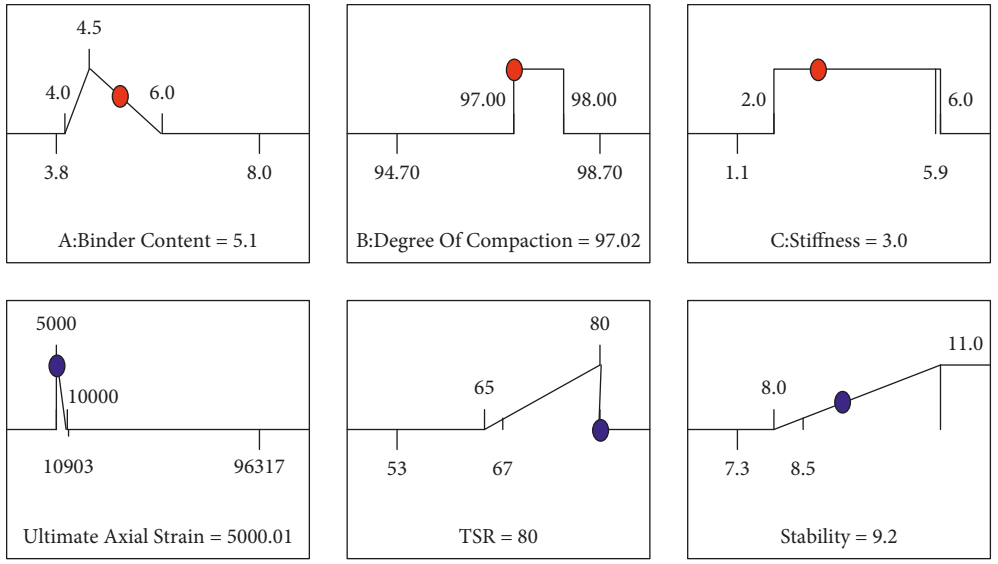

Figure 19: Optimum conditions and responses.

the stability of mixes. Meanwhile, increasing the binder content to more than 6% can lead to a reduction in the stability of mixes. Optimum stability values can be achieved when binder content is in the range of 4.7% to 5.9%. The surface plot indicated that the red region was produced when optimum binder content was achieved, while the degrees of compaction and stiffness, respectively, were at their highest. In general, excess binder content, a lower degree of compaction, and stiffness can result in lower stability of asphalt mixes.

The model was optimized to determine the factor conditions that provide maximum stability while achieving the target for axial strain and tensile strength ratio. All the factors and responses with their particular lower and upper limits were respecified for the optimum state and best resistance to pavement failure based on the PWD specifications. Figure 19 illustrates the predicted optimum conditions and the response in this study. The ultimate axial strain, tensile strength ratio, and stability that were predicted were found to be 5000 microstrains, 80%, and 9.2 kN, respectively.

4. Conclusions

The goal of the study is to investigate the current state of flexible pavements from laboratory testing that includes physical, volumetric, and performance tests on core samples. Based on the findings, the following conclusion has been reached:

(1) Samples C and D exhibited the highest degree of conformity to PWD specifications (the least severe condition), in contrast to Samples B and E, which exhibited severe conditions based on physical and volumetric tests.

(2) All the samples were susceptible to moisture damage, with Sample B having the most creep deformation and Sample D the least.

(3) Numerical optimization of an existing flexible pavement predicted optimum operation parameters for achieving a minimum ultimate axial strain (5000 microstrains), maximum tensile strength ratio (80%), and maximum stability (9.2 kN). The study revealed that the response surface methodology (RSM) is an effective statistical method for providing an appropriate empirical model for relating parameters and predicting the optimum performance of asphaltic mixture to reduce flexible pavement failure.

(4) Future research on the quality control of flexible pavement should be conducted using the findings of this study and field testing methods, such as the falling weight deflectometer (FWD) and the dynamic cone penetrometer (DCP), to determine the viability of flexible pavement in field conditions. Response surface method research should include more trial runs in the future to improve the process of optimization.

Data Availability

All the data used to support the findings of this study are included within the article.

Conflicts of Interest

The authors have no conflicts of interest.

Acknowledgments

Special thanks go to the Research Management Institute (RMI) of Universiti Teknologi MARA for providing the financial support under the FRGS (600-IRMI/FRGS 5/3(379/2019)). The authors would like to thank the School of Civil Engineering, College of Engineering, Universiti Teknologi Mara Shah Alam, Selangor for providing the experimental facilities and to all technicians at Highway and Traffic Engineering Laboratory.

References

[1] P. Cui, Y. Xiao, M. Fang, Z. Chen, M. Yi, and M. Li, "Residual fatigue properties of asphalt pavement after long-term field service," *Materials*, vol. 11, no. 6, pp. 1–3, 2018.

[2] NG. Sorum, T. Guite, and N. Martina, "Pavement distress: a case study," *Int J Innov Res Sci Eng Technol*, vol. 3, pp. 274–284, 2014.

[3] D. Day, I. M. Lancaster, and D. McKay, "Emulsion cold mix asphalt in the UK: a decade of site and laboratory experience," *Journal of Traffic and Transportation Engineering*, vol. 6, no. 4, pp. 359–365, 2019.

[4] Y. Darma, M. R. Karim, and S. Abdullah, "An analysis of Malaysia road traffic death distribution by road environment," *Sādhanā*, vol. 42, no. 9, pp. 1605–1615, 2017.

[5] D. Liu, M. Lin, and S. Li, "Real-time quality monitoring and control of highway compaction," *Automation in Construction*, vol. 62, pp. 114–123, 2016.

[6] G. Rada, D. Jones, and K. Senn, "A rational approach for conducting highway pavement forensic investigations," *International Journal of Forensic Engineering*, vol. 2, no. 3, p. 166, 2015.

[7] Z. Hossain, NH. Chowdhury, and A. Braham, "Forensic evaluation of premature pavement failures in Arkansas," *Journal of Performance of Constructed Facilities*, vol. 32, 2018.

[8] SS. Adlinge and AK. Gupta, "Pavement deterioration and its causes," *Int J Innov Res Dev*, vol. 2, pp. 437–450, 2013.

[9] H. Zelelew, K. Senn, and T. Papagiannakis, "Forensic evaluation of the LTPP specific pavement study projects in Arizona," *Journal of Performance of Constructed Facilities*, vol. 26, no. 5, pp. 668–678, 2012.

[10] S. A. F. Al-Arkawazi, "Flexible pavement evaluation: a case study," *Kurdistan Journal of Applied Research*, vol. 2, no. 3, pp. 292–301, 2017.

[11] A. Hosseini, A. Faheem, H. Titi, and S. Schwandt, "Evaluation of the long-term performance of flexible pavements with respect to production and construction quality control indicators," *Construction and Building Materials*, vol. 230, Article ID 116998, 2020.

[12] KS. Minhas, "Effect of binder content on volumetric properties of asphalt mix," *Elk Asia Pacific J Civ Eng Struct Dev*, vol. 5, 2019.

[13] R. Putra Jaya, KA. Masri, H. Awang, MI. Ali, NI. Ramli, WNA. Wan Azahar et al., "Stability and stiffness of asphaltic concrete incorporating waste cooking oil," *International Journal of Recent Technology and Engineering*, vol. 7, pp. 16–19, 2019.

[14] P. Jitsangiam, K. Nusit, and H. Nikraz, "An evaluation of moisture damage resistance of asphalt concrete based on dynamic creep characteristics," *KSCE Journal of Civil Engineering*, vol. 23, no. 4, pp. 1610–1616, 2019.

[15] SR. Omranian, MO. Hamzah, MRM. Hasan, and NH. Abdullah, "Evaluation of asphalt mixtures performance produced via drum and batch mixing plants," *Journal of Engineering Science & Technology*, vol. 14, pp. 2761–2778, 2019.

[16] D. Baskandi, "Influence of construction parameters on performance of dense graded bituminous mixes," *IOSR J Mech Civ Eng Ver III*, vol. 12, pp. 2320–2334, 2015.

[17] AM. Zaltuom, "A review study of the effect of air voids on asphalt pavement life," *Proceedings of First Conference for Engineering Sciences and Technology*, vol. 2, pp. 618–625, 2018.

[18] AEAEM. Behiry, "Laboratory evaluation of resistance to moisture damage in asphalt mixtures," *Ain Shams Engineering Journal*, vol. 4, no. 3, pp. 351–363, 2013.

[19] S. Ismail, N. Abdul Hassan, H. Yaacob et al., "Properties of dense-graded asphalt mixture compacted at different temperatures," *IOP Conference Series: Earth and Environmental Science*, vol. 220, 2019.

[20] MO. Hamzah, B. Golchin, and CT. Tye, "Determination of the optimum binder content of warm mix asphalt incorporating rediset using response surface method," *Construction and Building Materials*, vol. 47, pp. 1328–1336, 2013.

[21] M. Soltani, TB. Moghaddam, MR. Karim, and H. Baaj, "Analysis of fatigue properties of unmodified and polyethylene terephthalate modified asphalt mixtures using response surface methodology," *Engineering Failure Analysis*, vol. 58, pp. 238–248, 2015.

[22] I. Tharazi, A. B. Sulong, F. M. Salleh, A. H. Abdullah, and N. F. Ismail, "Application of response surface methodology for parameters optimization in hot pressing kenaf reinforced biocomposites," *Journal of Mechanical Engineering*, vol. 17, no. 3, pp. 131–144, 2020.

[23] A. I. Nassar, N. Thom, and T. Parry, "Optimizing the mix design of cold bitumen emulsion mixtures using response surface methodology," *Construction and Building Materials*, vol. 104, no. 0, pp. 216–229, 2016.

[24] J. Ahmad, Md. Yusoff. Ni, MR. Hainin, MY. Abd Rahman, and M. Hossain, "Evaluation on performance characteristics of superpave asphalt mix design under tropical climatic conditions," *Int J Pavement Res Technol*, vol. 7, no. 5, pp. 331–342, 2014.

[25] FM. Jakarni, MF. Rosli, Md. Yusoff. Ni, MMA. Aziz, R. Muniandy, and S. Hassim, "An overview of moisture damage performance tests on asphalt mixtures," *J Teknol*, vol. 78, pp. 91–98, 2016.

[26] Z. Jeirani, B. Mohamed Jan, B. Si Ali, I. M. Noor, C. H. See, and W. Saphanuchart, "Prediction of the optimum aqueous phase composition of a triglyceride microemulsion using response surface methodology," *Journal of Industrial and Engineering Chemistry*, vol. 19, pp. 1304–1309, 2013.

[27] E. Sengul Celaleddin, O. Seref, E. Iskender, and A. Aksoy, "Evaluation of SBS modified stone mastic asphalt pavement performance," *Construction and Building Materials*, vol. 41, pp. 777–783, 2013.

[28] E. Iskender and A. Aksoy, "Field and laboratory performance comparison for asphalt mixtures with different moisture conditioning systems," *Construction and Building Materials*, vol. 27, pp. 45–53, 2012.

[29] MO. Hamzah and SR. Omranian, "Effects of short term aging on dynamic creep properties of asphalt mixtures," *J Teknol*, vol. 76, 2015.

[30] J. Ahmad, MYA. Rahman, MR. Hainin, and M. Hossain, "Comparative evaluation of hot-mix asphalt design methods," *International Journal of Pavement Engineering*, vol. 13, pp. 89–97, 2012.

[31] AM. Alnadish and YM. Aman, "Mechanistic approach for reducing the thickness of asphalt layer incorporating steel slag aggregate," *Civil Engineering J*, vol. 4, p. 334, 2018.

[32] Y. Niazi and M. Kalili, "Effect of Portland cement and lime additives on properties of cold in place recycled mixtures with asphalt emulsion," *Construction and Building Materials*, vol. 23, pp. 1338–1343, 2009.